

Vineet Vishwakarma*, Sara Marchini, Eckhard Schleicher, Markus Schubert* and Uwe Hampel

A framework for validating efficiency models of thermal separation columns with tray internals

<https://doi.org/10.1515/cppm-2024-0037>

Received May 16, 2024; accepted November 19, 2024; published online December 18, 2024

Abstract: Tray columns are globally used for distillation processes, and their performance must be optimized to reduce their cost and energy expenditures as well as carbon emissions. A prerequisite to achieve these targets demands a realistic account of the tray performance based on tray efficiency model application. The proof of concept of a Refined Residence Time Distribution (RRTD) model, recently proposed by the authors, is presented. The multifaceted challenges in acquiring hydrodynamic and performance data suitable for model validation are discussed in this work. In that regard, an unprecedented experimental campaign was performed in a representative large-scale air-water tray column simulator based on the application of multiplex flow profiler, new chemical system, and novel data processing schemes. Using these data and additional case studies, the capabilities of the RRTD model were demonstrated. This model successfully accounted for the impacts of varying local liquid flow characteristics and vapor flow maldistributions on the tray efficiency thereby advancing the state of the art of the tray efficiency models. This work particularly aimed at proposing a constructive framework to evaluate tray efficiency models in the future campaigns, and those campaigns will benefit from the learnings of the present work.

Keywords: tray column; Murphree efficiency; mathematical model; residence time distribution; two-phase hydrodynamics; gas stripping

1 Introduction

Distillation is the leading thermal separation technology that constitutes around 95 % of all separations in chemical process industries [1]. Industrial separations are carried out in large columns, and half of such columns worldwide are estimated to be equipped with trays [2]. Despite their enormous cost and energy requirements, these columns continue to be in service due to the lack of any industrially viable alternative [3, 4]. Today, increasing energy costs and alarming emergency to control greenhouse gas emissions urgently compel to improve columns' separation performance. This can be achieved by improving the performances of individual trays, since such columns are generally regarded as the cascades of trays with similar geometries and functions [5]. This notion demands an

Note: Manuscript for special issue honoring Prof. Dr.-Ing. Eugeny Kenig in Chemical Product and Process Modeling (CPPM).

***Corresponding authors: Vineet Vishwakarma**, Department of Mechanical Engineering, The Pennsylvania State University, University Park 16802, PA, USA, E-mail: vxv5175@psu.edu. <https://orcid.org/0000-0002-5428-4112> (V. Vishwakarma); and **Markus Schubert**, Chair of Chemical Process Engineering, Technische Universität Dresden, Dresden 01062, Germany; and Institute of Fluid Dynamics, Helmholtz-Zentrum Dresden-Rossendorf, Bautzner Landstraße 400, 01328 Dresden, Germany, E-mail: markus.schubert@tu-dresden.de

Sara Marchini, Chair of Chemical Process Engineering, Technische Universität Dresden, Dresden 01062, Germany; and Institute of Fluid Dynamics, Helmholtz-Zentrum Dresden-Rossendorf, Bautzner Landstraße 400, 01328 Dresden, Germany

Eckhard Schleicher, Institute of Fluid Dynamics, Helmholtz-Zentrum Dresden-Rossendorf, Bautzner Landstraße 400, 01328 Dresden, Germany

Uwe Hampel, Institute of Fluid Dynamics, Helmholtz-Zentrum Dresden-Rossendorf, Bautzner Landstraße 400, 01328 Dresden, Germany; and Chair of Imaging Techniques in Energy and Process Engineering, Technische Universität Dresden, 01062 Dresden, Germany

accurate account of the individual tray performance first, which is traditionally expressed in terms of the Murphree vapor-side tray efficiency (E_{MV}) as

$$E_{MV} = \frac{\bar{y}_{out} - \bar{y}_{in}}{\bar{y}_{out}^* - \bar{y}_{in}} \quad (1)$$

In Eq. (1), \bar{y}_{in} and \bar{y}_{out} are the average mole fractions of a particular component in the vapor¹ stream entering and exiting a tray, respectively. Here, \bar{y}_{out}^* denotes the mole fraction of that component in the vapor phase, which would be in equilibrium with the liquid phase of the same component exiting that tray. Another efficiency definition relevant to the trays is the Murphree vapor-side point efficiency (E_{OV}), which is defined as

$$E_{OV} = \frac{y_p - \bar{y}_{in}}{y_p^* - \bar{y}_{in}} \quad (2)$$

In Eq. (2), y_p is the mole fraction of a component in the vapor that leaves from an arbitrary point ‘p’ on the tray, whereas y_p^* refers to the mole fraction of the same component in the vapor that would be in equilibrium with the liquid at that point. The point efficiency can vary over a tray depending on the liquid concentration gradient present on that tray [6]. Still, the point efficiency is generally considered to be uniform over a tray in the modeling of tray and column efficiencies. E_{MV} is usually greater than E_{OV} , and the former can exceed unity owing to concentration gradient in the liquid along the flow path [7]. Analogous definitions of given efficiencies also exist for the liquid phase although they are generally not used to indicate tray performances.

It is long known that the tray efficiency is significantly affected by the flow and mixing patterns of liquid and vapor in the two-phase dispersion above the tray [8, 9]. The plug flow of liquid and vapor are considered ideal for tray performance. However, the non-ideal flow profiles such as channeling and bypassing (both in liquid and vapor), recirculation and stagnant zones (only in the liquid phase) are detrimental to the tray efficiency [10]. The impact of such liquid profiles on the tray efficiency can be predicted by the so-called tray efficiency models [11]. Moreover, it is postulated that maximizing the tray efficiency is possible by optimizing the flow and mixing characteristics of the two-phase dispersion via design modifications and revamps. Such optimization can be achieved by strategically iterating tray designs and revamps with respect to the resulting efficiencies based on the application of tray efficiency models. Therefore, a realistic tray efficiency model capable of predicting accurate efficiencies should be at hand, and the corresponding predictions must confirm the efficiencies obtained experimentally. The existing models in literature suffer from several key limitations, whereas their validation based on experiments has generally remained challenging.

The aim of this work is to present an unprecedented framework for direct experimental assessment of an advanced tray efficiency model. First, the limitations of the existing models followed by recent development of an advanced model targeting those limitations are discussed in Section 2. In that section, the technological challenges involved in the validation of tray efficiency models are also revisited briefly, and the parameters of interest pertaining to two-phase hydrodynamics and mass transfer performance for advanced model validation are introduced. Then, the particulars of a constructive framework comprising of a sophisticated multiplex flow profiler, new chemical system, and novel data processing schemes are described in Section 3 along with their application in a representative large-scale air-water tray column simulator for hydrodynamic and performance data acquisition. Based on the recorded experimental data as well as supporting case studies, the superiority of the advanced tray efficiency model is evaluated in Section 4 by comparing its predictions with those of the existing models. Section 5 provides concluding remarks on the utility of this work for realistic assessment of tray performance as well as for checking the applicability of the models predicting fluid dynamics and tray efficiency. Furthermore, the authors acknowledge the multifaceted challenges involved in the experimental assessment of tray efficiency models, which are difficult to address altogether. Thus, it was necessary for the authors to refer to their recent progress on this topic for reasonably demonstrating direct validation and assessment of the tray efficiency models.

¹ The ‘vapor’ and ‘gas’ terms are used interchangeably in this work.

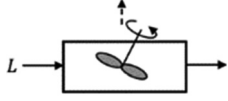
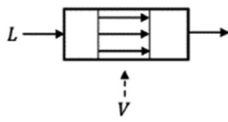
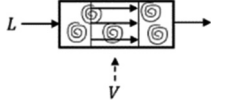
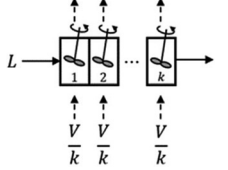
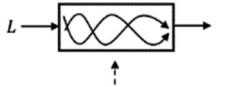
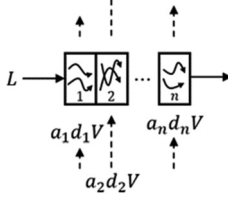
2 An overview of the tray efficiency models and general challenges in their validation

The development of tray efficiency models basically relied on the analyses of two-phase flow, crossflow hydraulics and mass transfer over the trays [12]. Depending on their formulation, these models state E_{MV} as a function of E_{OV} and other parameters such as stripping factor (λ), Péclet number (Pe), number of perfectly mixed liquid cells along the flow path (k), and so forth. The stripping factor is a system parameter, which is the ratio of the slopes of vapor-liquid equilibrium (VLE) line and operating line (i.e., determined from the VLE data and tray loadings, respectively). According to their respective accounts of individual liquid and gas flows, the existing models and their schemes are summarized in Table 1. The perfectly mixed model (Eq. (3)) and the plug flow model (Eq. (4)) [13] are the basic models, where the liquid on the tray is assumed to be completely mixed and completely unmixed (longitudinally), respectively. On the other hand, more realistic models consider partial liquid mixing along the flow path on a tray in terms of Pe , k and $f(t)$ (i.e., residence time distribution (RTD) function) in the AIChE model (Eq. (5)) [14], mixed stages model (Eq. (6)) [15] and RTD model (Eq. (7)) [16], respectively (refer to Table 1). Here, Pe and k point to liquid mixing in the respective models [17], whereas $f(t)$ refers to the liquid flow behavior with combined effects of both eddy mixing and velocity gradients [18]. The mixing parameters stated earlier can be derived from this function. The general assumptions in these models include constant point efficiency, linear VLE, vapor plug flow with perfect mixing between the trays, and uniform dispersion height in some models. Among more realistic models, the AIChE model has received the most recognition (finding its way into the acclaimed AIChE's bubble tray design manual (1958)) owing to its simplicity. However, the RTD model remained the most realistic one among the practical models because of its ability to account for different degrees of liquid maldistribution [16]. The feasibility of the stimulus-response experiments in general makes the application of the RTD model practicable. A collective formulation and assessment of the existing models (including a few of those not mentioned here) and corresponding validation schemes can be found elsewhere [11].

The existing models suffer from two prominent limitations that should be addressed for better estimation of the tray performance. First, those models rely on parameters such as liquid Péclet number, number of perfectly mixed liquid cells, etc. that are usually retrieved based on tracer sampling at the tray outlet (refer to model schematics in Table 1). This suggests the consideration of a homogeneous liquid flow characterized by the given parameters in those models. This is contrary to the real scenario, where liquid flow characteristics may vary over a tray deck due to the agitation caused by rising vapor, dispersion as well as expanding and contracting flow path in the column cross-section [20]. In principle, such models disregard local flow variations in the liquid phase and consider the tray as a black box for efficiency predictions. The second key limitation is the ignorance of such models to any vapor flow maldistribution. As a compromise, uniform and unidirectional flow of vapor is assumed unanimously in the existing models, which is also evident in their schematics in Table 1. This assumption may hold either for a small tray or the lowest tray in a column next to reboiler, however, it is certainly invalid for a large tray due to its long flow path [17, 21]. According to [22]; excessive hydraulic gradients in the liquid phase on a tray leads to non-uniform vapor distribution, and vice-versa. To the best of the authors' knowledge, only few studies [21–23] attempted incorporating vapor flow maldistribution in the eddy diffusion concept for tray efficiency predictions, but they remained largely focused on examining tray efficiencies for either perfectly mixed liquid or liquid plug flow during non-uniform vapor distribution. Even for these theoretical cases of the liquid flow, the referred studies provided contradicting observations about the impact of vapor flow maldistribution on the tray efficiency, which demanded further investigation.

To overcome the limitations of the existing tray efficiency models and eventually propose an advanced model, we first geometrically discretized a tray into a series of compartments along the flow path (see Table 1) [19]. In this new model, each compartment (i.e., characterized by its area fraction (a)) was assumed to operate as an individual tray with distinct RTD function and separation efficiency according to the conventional RTD model. Then, the compartment efficiencies were interlinked with the overall tray efficiency through integral transform and system theory resulting in a new model referred to as the Refined RTD (RRTD) model (Eq. (8)). The RRTD

Table 1: Synopsis of the tray efficiency models proposed in the literature.

Reference	Schematic	Model and parameters
Perfectly mixed model		$E_{MV} = E_{OV}$ (3)
Plug flow model [13]		$E_{MV} = \frac{e^{(\lambda E_{OV} - 1)}}{\lambda}$ (4)
AIChE model [16]		$\frac{E_{MV}}{E_{OV}} = \frac{1 - e^{-(\eta + Pe)}}{(\eta + Pe) \left(1 + \frac{\eta + Pe}{\eta}\right)} + \frac{e^{\eta} - 1}{\eta \left(1 + \frac{\eta}{\eta + Pe}\right)}$ (5)
Mixed stages model [15]		$E_{MV} = \frac{\left(1 + \frac{\lambda E_{OV}}{k}\right)^k - 1}{\lambda}$ (6)
RTD model [16]		$E_{MV} = \frac{1 - \int_0^{\infty} e^{-\lambda E_{OV} t / \tau} \cdot f(t) dt}{\lambda \int_0^{\infty} e^{-\lambda E_{OV} t / \tau} \cdot f(t) dt}$ (7)
RRTD model [19]		$E_{MV} = \frac{\left[\prod_{i=1}^n (1 + \alpha_i d_i \lambda E_{MV, i}) \right] - 1}{\lambda}$ (8)

Here, $\eta = 0.5 \cdot Pe \{ \sqrt{1 + (4\lambda E_{OV}/Pe)} - 1 \}$. Other parameters are defined in the text.

model ensures the contribution of the local dynamics of the evolving liquid phase on the overall tray performance via compartment efficiencies, which addresses the concern of previous black box efficiency predictions. The discretization scheme in the RRTD model also permits considering different vapor flow in the compartments (i.e., vapor flow maldistribution) through their vapor allocation indices (d) for efficiency predictions. These arguments clearly state the advancements in the tray efficiency modeling achieved by the RRTD model. Initial verification of the RRTD model involved separately analyzing the tray efficiencies for perfectly mixed and plug flow of liquid in the compartments with vapor plug flow through the tray. For these conditions, the RRTD model correctly transformed into mixed stages model and plug flow model, respectively (see Table 1 for reference). The RRTD model transformation into the plug flow model was also verified for any arbitrary distribution of vapor flow through the tray, which proved the corresponding claims of [21] and [23]. Full description of the RRTD model formulation and related assumptions are available elsewhere [24]. It should be noted that the RRTD model has not been validated so far due to the unavailability of the high-resolution two-phase flow and mass transfer data pertaining to an operational column tray.

The general requirements for validating any tray efficiency model include hydrodynamic and mass transfer data of an operational column tray. With reference to Table 1, the hydrodynamic data correspond to $f(t)$ and $\tau (= \int_0^\infty t f(t) dt$, i.e., liquid mean residence time), Pe and k (depending on the model preference) at selected liquid (L) and vapor (V) flow rates. As this work aims to experimentally validate the new RRTD model, the liquid RTD functions and residence times related to the compartment flow domains and the entire tray were targeted within the froth dispersion, as often encountered in industrial columns [25]. To do so, it is required to identify the effective froth height followed by the underlying distributions of liquid holdup and tracer concentration as demonstrated in Figure 1. This would be sufficient for the application of the tray efficiency models provided they are complemented with VLE slope and point efficiency data. The complementary data and the actual tray efficiency (for model validation) constitute the performance data usually obtained via species transfer between phases by applying a suitable chemical system. The chaotic and 3D nature of froth dispersion [26, 27] and the limitations posed by traditional measurement techniques and chemical systems [28, 29] make acquiring the hydrodynamic and performance data very challenging.

Non-invasive techniques such as γ -ray densitometry [30–35] and γ -ray computed tomography [36–39] have been used in the past for studying local froth characteristics and process monitoring (including column troubleshooting), respectively. Few studies employed probe techniques (such as those based on conductivity and light transmission) to investigate local bubble characteristics in the froth above the tray [34, 40, 41]. Overall, 3D accesses to the tray hydrodynamics including froth height and liquid holdup on large-scale trays remained impossible so far, and compromisingly, many studies resorted to visual estimation of such heights. Further, liquid flow monitoring on trays via tracer has traditionally relied on either point measurements via fiber-optic probes [42], conductivity probes [43], wire-mesh sensor [9] or camera techniques such as photographic [44] and infrared imaging [10]. The point measurement techniques (without any tracer) employed in this regard also included strain gauge probes [45], thermocouples [46], hot film anemometer [47] and thermometers [48]. Despite being reasonably successful in revealing gross liquid maldistribution, the camera techniques are only good for the near surface visualizations, whereas probe measurements often require complicated calibration procedures and suffer from low spatial resolution, substantial signal interference, complex electronic schemes, and highly invasive behavior. A thorough review of these techniques and their application on column trays can be found elsewhere [11].

Air-water column simulators are popular among suppliers and vendors of column internals for hydrodynamic evaluations. Acquiring separation performance data from those simulators generally demands the application of a chemical system followed by species concentration analysis using a recognized measurement technique. For convenience, the systems applied in the past are classified into four categories namely gas stripping systems (air– O_2 +water [49], air– NH_3 +water [50]), gas absorption systems (NH_3 +air–water [51], CO_2 +air–water [52]), air humidification system (air–water [53, 54]) and organic distillation systems (cyclohexane–n-heptane [55, 56], methanol–water [57]). Few common systems pertaining to each category are also provided in parentheses for reference. Low gas solubility in stripping systems makes them inapplicable for large trays, whereas using gases like NH_3 , CO_2 , SO_2 etc. in both absorption and stripping systems pose severe health and safety

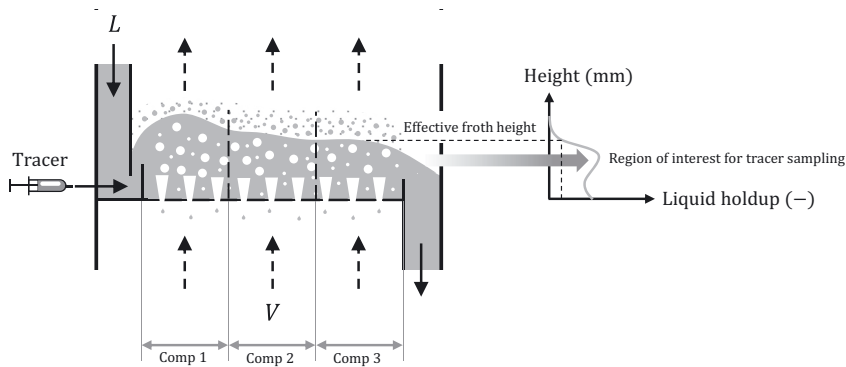


Figure 1: Illustration for hydrodynamic characterization of a column tray that is geometrically discretized into compartments for the RRTD model validation.

hazards and require effluent conditioning and treatment. Precise air conditioning and monitoring needed for humidification systems challenges their integration in column simulators. The organic distillation systems demand industrial-scale facilities that can process inherently hazardous mixtures usually at higher temperature and pressure. In the latter, getting relevant hydrodynamic data for model validation is not even feasible although their performance data would be highly relevant for the industry [58]. Furthermore, using a small tray [16] or a small-scale Oldershaw column [59]) is common for measuring point efficiencies, although their wall effects and flow characteristics can be significantly different from those of large trays. Other general approaches to determine point efficiencies include (i) back calculation through tray efficiency model application in cases with predetermined tray efficiency and mixing parameter, and (ii) calculation via number of transfer units based on correlations and mass balances. Further description of the existing systems including their specifications and drawbacks are available elsewhere [28].

3 Advanced experimental campaign for validating tray efficiency models

This section describes the comprehensive experimental campaign undertaken to generate unprecedented hydrodynamic and performance data and validate the new RRTD model.

3.1 Framework for hydrodynamic data acquisition

3.1.1 Experimental facility and imaging technique

An air-water column simulator (DN800) housing two sieve trays (each with 3,052 holes of 5 mm diameter) was built to obtain high-resolution hydrodynamic data for the RRTD model validation. The schematic diagram of the

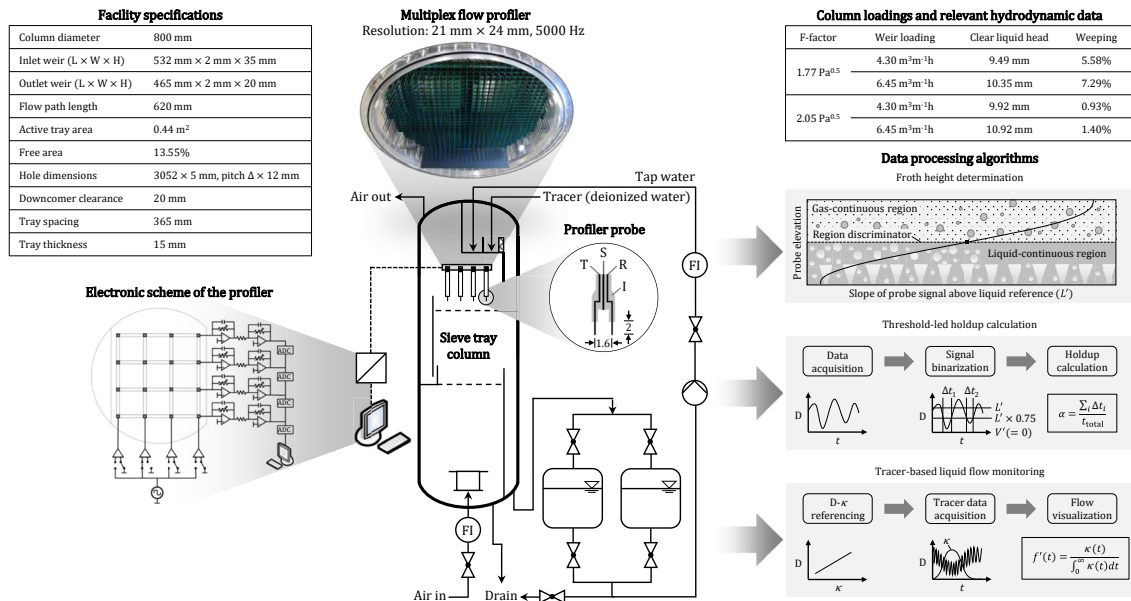


Figure 2: Description of the experimental setup and measurement technique (center) for hydrodynamic characterization of the two-phase dispersion over sieve tray along with technical specifications of the facility (top left), electronic scheme of the profiler exemplified for a 4 × 4 probe arrangement (left middle), column loadings (top right) and data processing algorithms (right). (D – probe data, FI – flow indicator, $f(t)$ – appearance time distribution function, I – insulation, L' – liquid-only probe signal, R – receiver, S – shielding, T – transmitter, t – time, V' – gas-only probe signal, α – time-averaged liquid holdup, and κ – liquid conductivity).

constructed facility and its technical specifications are presented in Figure 2 (middle and top left). As shown in this figure, pressurized air was introduced to the column from the bottom, whereas tap water was pumped to the column top. The tap water flowed downward in the column along a zigzag path and interacted with the air rising through tray perforations. The resulting froth on the top tray (see Figure 2 (middle)) was targeted for the hydrodynamic characterization. Based on preliminary tests, the weir loadings (i.e., liquid flow rate per outlet weir length) in the column were selected as $4.30 \text{ m}^3 \text{ m}^{-1} \text{ h}^{-1}$ and $6.45 \text{ m}^3 \text{ m}^{-1} \text{ h}^{-1}$, whereas gas loadings in terms of F -factors of $1.77 \text{ Pa}^{0.5}$ and $2.05 \text{ Pa}^{0.5}$ were considered. At these loadings, the liquid weeping from the tray (i.e., measured via weeping collection) and the clear liquid heights (based on the gas momentum and capillary rise corrections of the time-averaged manometric heads [60]) were obtained as given in Figure 2 (top right). Due to its low electrical conductivity, a predefined pulse of deionized water as a tracer was later injected prior to the inlet weir of the top tray for flow monitoring. The full scheme of the facility including instrumentation and auxiliary equipments are separately available [61].

To visualize froth characteristics on column trays, the authors developed and patented a multiplex flow profiler as shown in Figure 2 (top middle) [62]. The skeletal grid of the profiler held 776 probes together in a 28×32 arrangement, where the inter-probe distances were 21 mm and 24 mm along the longitudinal (i.e., flow-wise) and transverse directions, respectively. Each probe concealed three different electrodes namely transmitter, receiver and shielding in an insulating sheath as depicted in Figure 2 (middle). Only the tips of the transmitter and receiver electrodes were exposed to the two-phase flow, whereas the insulation and shielding electrode minimized the effects of crosstalk and capacitance buildup. Figure 2 (left middle) also exemplifies the electronic scheme of the profiler, which was adapted from the standard Teletronic WMS 200 system [63]. Based on the presented scheme in this figure, the transmitters of each probe along a column (i.e., in transverse direction) were applied with an excitation voltage, simultaneously, and then each column probes were activated serially via multiplexing scheme. Depending on the local instantaneous conductance near the probe tips, the electric current measured by all receivers were sampled, parallelly, followed by amplification and digitization for data processing. The sampling frequency of the profiler in this work was 5,000 Hz. Accordingly, the profiler probes discerned the temporal variations of the phases near the probe tips (i.e., essential for holdup and froth height calculations). The profiler probes identified the temporal changes in the electrical conductivity caused by tracer near their tips (i.e., necessary for flow visualization via RTD analysis). The entire profiler assembly was suspended over the top tray using a height-adjustable aluminum frame (not shown here). This profiler made the high-resolution 3D imaging of the two-phase dispersion on trays possible for the first time. Full details of geometry and features of the probes as well as profiler's electronic scheme can be found in a separate article [61].

3.1.2 Data acquisition, processing, and visualization

The data acquisition for quantifying the distributions of liquid holdup and froth height at selected weir loadings and F -factors started by immersing the profiler probes in the two-phase dispersion once the column attained steady state. The probe measurements were performed for 300 s at each height between 20 mm and 100 mm elevations above the tray in increments of 10 mm. The 20 mm high liquid sampling taps above tray deck (for mass transfer measurements; refer to Section 3.2) restricted lowering the profiler probes further. As illustrated in Figure 2 (right middle), a single threshold technique was employed to binarize the two-phase digital data into individual gas and liquid exposures and to calculate the time-averaged liquid holdup at every probe location. How to find the best threshold level for relevant probe tip measurements was demonstrated by [29] using γ -ray computed tomography. To filter out the holdup data via froth height identification, the probe responses were analyzed according to the local phase continuity and the so-called geometry factor of the tips [64]. In simple terms, any gas volume approaching a probe in the liquid-continuous dispersion would reduce the geometry factor as well as the transferred current between the tips prior to the gas-only signal (i.e., zero) once that volume encapsulates the probe tips. In the gas-continuous dispersion, the liquid accumulation and descent on the probe shaft due to gravity would increase the geometry factor between the tips (causing a rise in the received signal) before falling off. Combining these facts with characteristic probe signals of each region, the average slopes of those signals were found to be negative and positive in the liquid-continuous and gas-continuous regions,

respectively (see Figure 2 (right middle)). The local effective froth height corresponding to each probe was the one with an average slope value of zero. By applying these approaches, 3D distributions of liquid holdup and upper froth boundary were obtained as shown for the selected heights in Figure 3a. The holdup masking above froth height (indicated by blue pixels) allowed computing the real liquid content in the froth as given by the average liquid holdups (see Figure 3a). Because of the gas-led liquid suspension above the deck, the liquid holdup increased with height until the upper froth boundary and reduced sharply to zero afterwards. In the tracer-based experiments, the tips of the profiler probes were set at 40 mm elevation above the tray due to reasonably homogeneous distributions of liquid holdup there (see Figure 3a). At the same operational settings of column and profiler, a linear relation between probe signal and electrical conductivity was established for each probe by prior exposure to liquids of different electrical conductivities (i.e., for the range expected during tracer experiments). Then, a 2s-pulse of tracer was introduced before the inlet weir, and corresponding changes in the electrical conductivity of the liquid within two-phase froth were monitored for 60 s. The recorded data were filtered and processed (refer to Figure 2 (right bottom)) to get the distributions of the mean tracer appearance time ($\bar{\tau} = \int_0^{\infty} t f'(t) dt$) shown in Figure 3b (left). It refers to the average time taken by the tracer to appear at probe tips after injection. The unidirectional liquid velocities calculated from these distributions are also presented in Figure 3b (left). Eventually, $f(t)$, τ , and Pe as provided for each case in Figure 3b (right) were computed for the entire tray by averaging conductivity profiles at the tray boundaries as

$$\bar{\kappa}(t) = \frac{\sum_{i=1}^j \alpha_i \kappa_i(t) / \tau_i}{\sum_{i=1}^j \alpha_i / \tau_i} \quad (9)$$

and performing deconvolution calculations using axial dispersion model. In Eq. (9), i and j refer to the probe index and the total number of probes along the tray boundary, respectively. The first two probe columns were

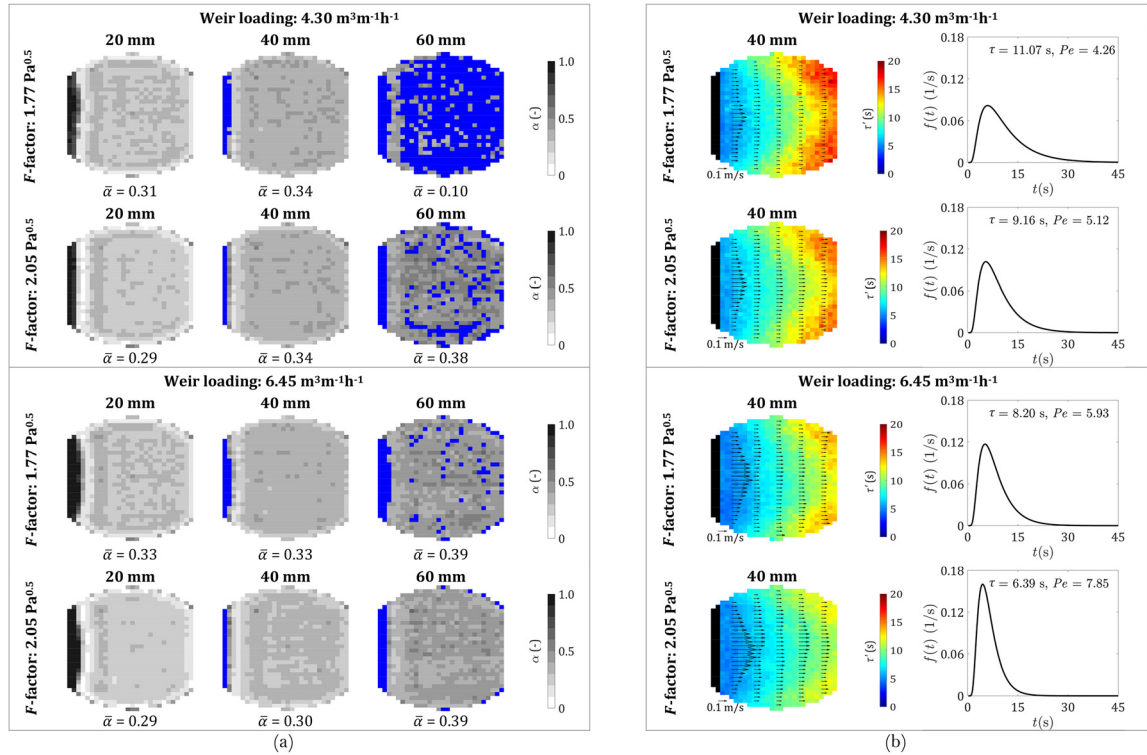


Figure 3: Distributions of (a) liquid holdup (α) and their mean values ($\bar{\alpha}$), and (b) tracer appearance time (τ) with unidirectional velocity including RTD function ($f(t)$), mean residence time (τ), and Péclet number (Pe) at selected elevations above the tray for given loadings. Blue pixels in (a) mask the holdups above the local froth heights, whereas black pixels in (b) indicate the probe data that were neglected in the respective calculations.

disregarded in the tracer-based calculations due to holdup masking there (refer to Figure 3a). The overall dependence of the RTD parameters on weir loadings and F -factors are self-explanatory in Figure 3b. In this figure, higher liquid velocities with parabolic distributions were observed in the first quarter along the flow path. Thereafter, the liquid velocities reduced and homogenized due to the agitating action of the upflowing gas. Full description of the experiments and data processing approaches from this section including the evidences of excellent data reproducibility, correctness of deconvolution calculations, and low uncertainties are available elsewhere [24].

3.2 Framework for performance data acquisition

3.2.1 Applied chemical system and analytical technique

The method of isobutyl acetate ($C_6H_{12}O_2$) stripping from its aqueous solution by air was applied in this campaign for direct measurements of tray and point efficiencies and stripping factor calculations [28, 65]. $C_6H_{12}O_2$ is a transparent solvent with fruity odor and has moderate solubility in water. Compared to previous systems reviewed in Section 2, the applied system is safe, cost-effective, and straightforward to implement in existing air-water column simulators as exemplified in Figure 4 (left) using the identical column facility and peripherals from Section 3.1. An aqueous solution batch with 400 ppm concentration of isobutyl acetate (prepared using deionized water) was sufficient to have measurable concentrations on both trays. The physical properties of the batch were identical with those of deionized water. It should be noted that the batch concentration can be adjusted depending upon the column size and operating conditions thereby referring to its application versatility. In this part of the campaign, the column operated identically as in Section 3.1 with the same weir loadings and F -factors. Before exiting the column, the air stripped out some of $C_6H_{12}O_2$ from the aqueous solution depending on the interfacial contact, which resulted in the distribution of species concentration over the top tray. To measure that concentration, 20 mm-high sampling taps were positioned equidistantly from each other on one half of the top tray (see Figure 4 (top middle)). Due to reasonable flow symmetry across the tray centerline (refer to Figure 3), only one half of the tray was considered for liquid sampling. Tap openings at 20 mm height above the tray permitted sample collection from the liquid-rich part of the froth.

The liquid samples collected from the tray column were analyzed via UV spectroscopy. Using Beer–Lambert law, the concentrations of isobutyl acetate in the collected liquid samples were obtained. As shown in Figure 4 (top right), the reference measurements allowed establishing a linear relation between concentration and absorbance at different wavelengths. After selecting a suitable wavelength, the light absorbance related to an actual sample from a tap provided the actual concentration of the isobutyl acetate. The concentration distributions presented in Figure 4 (middle) were acquired by applying polynomial fitting on the respective data at given tap locations. The distributions of the species concentration in Figure 4 (middle) follow similar trends as those of the tracer appearance time from Figure 3b (left). It should be noted that – depending on the operating condition – the batch liquid spent different time in the flow loop before arriving at the tray inlet and had minor variation in the batch specification. Hence, achieving a fixed species concentration before inlet was challenging, and any tap-to-tap comparison of the concentration is not recommended. However, this is insignificant for the efficiency calculations that are based on the difference in the concentration values. The overall approach discussed in this section considered the presence of both liquid- and gas-side mass transfer resistances and may not be suitable to find individual liquid- and gas-phase mass transfer coefficients. Nonetheless, it is suitable to get desired performance data for validating tray efficiency models, and thus, is recommended for similar purpose in future campaigns. Individual accounts of the phase resistances, the proof of negligible effect of the hydrolysis reaction of isobutyl acetate in dilute solution, and data reproducibility ensured via multiple experimental runs can be found elsewhere [28].

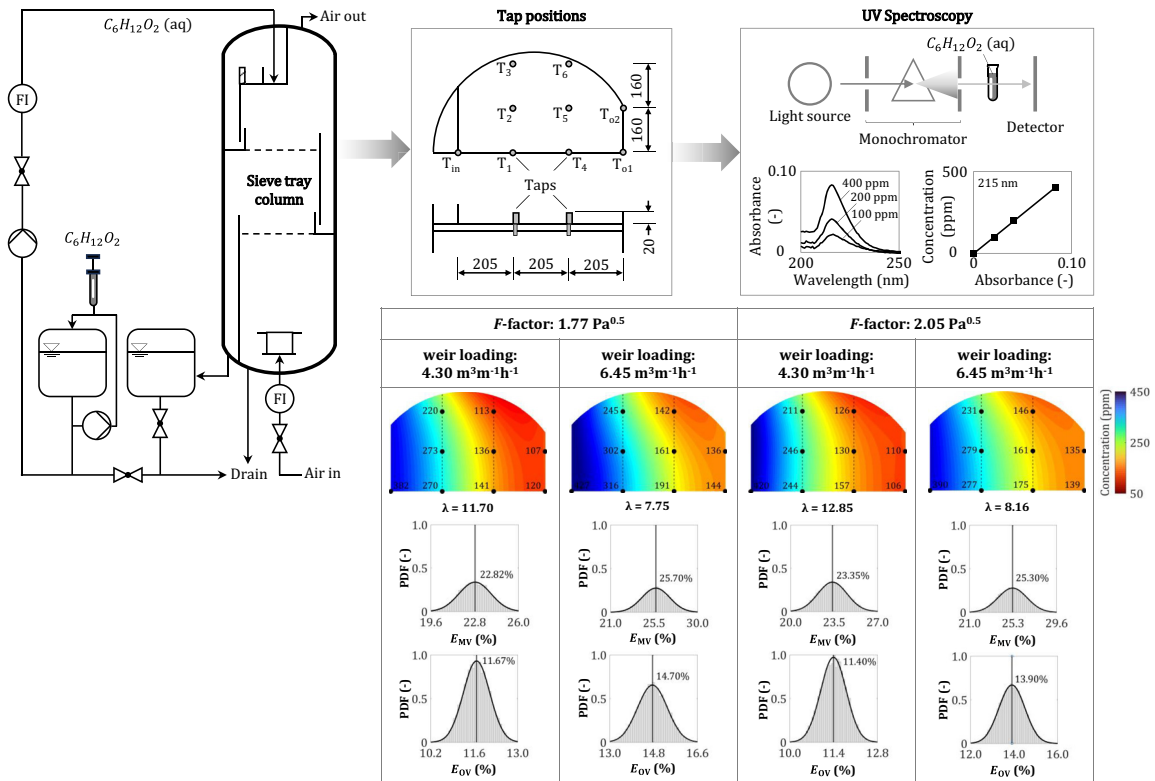


Figure 4: Adaptation of the experimental setup (left) for performance assessment including tap positions (top middle: not drawn to scale), UV spectroscopy technique (top right), concentration distributions of isobutyl acetate (aq) and performance data (mid-bottom).

3.2.2 Data processing and performance analysis

The liquid-side tray efficiencies were calculated from the species concentrations along the tray boundaries for the given operating conditions. To do so as well as to calculate stripping factors, the species concentration in the liquid phase that would be in equilibrium with its counterpart in the exiting gas was computed by supplementing Henry's law with liquid temperature and total gas pressure for each condition. Then, the vapor-side tray efficiencies were obtained via material balancing on the tray. From tray efficiency, the point efficiency (i.e., assumed constant for the tray) was acquired by integrating liquid concentrations over the tray for each condition. As point efficiency is a weak function of the superficial gas velocity, it can be assumed constant irrespective of any gas flow maldistribution, which simplifies the efficiency calculations [21]. The VLE was also considered to be linear in the efficiency and stripping factor calculations.

Minor variations in absorbance data of the liquid samples were observed due to local concentration fluctuations, inherent uncertainties of the spectroscopy technique, and fluctuations in the sample temperature. Those variations must be accounted for in the concentration distributions and resulting efficiencies. The temperature fluctuations in both liquid and gas influence the stripping factor data. Multiple experimental runs were performed mainly to quantify maximum variations in the absorbance and temperature data. Accordingly, 10 thousand cases of species concentration distributions were generated by considering randomly distributed errors in the parametric values, which guaranteed the confidence levels greater than 95 % on the obtained efficiency distributions. The resulting probability density functions (PDF) of the tray and points efficiencies are depicted in Figure 4 (bottom) for all operating conditions. The mean values of those efficiencies as well as stripping factor data form the basis of the model validation, whereas maximum standard deviations in the tray and point efficiencies in this campaign were 1.44 % and 0.61 %, respectively. A direct comparison of the efficiency data is only meaningful when the E_{MV}/E_{OV} values are available at same λE_{OV} along with the RTD parameters.

Further description on how to retrieve the performance data including overall uncertainties can be found elsewhere [28].

4 Evaluation of the predictive capabilities of the tray efficiency models

4.1 Model examination based on experimental data

The hydrodynamic and performance data presented so far generally suffice for evaluating the predictions from a tray efficiency model. To validate the RRTD model regarding longitudinal variations in the liquid mixing, the tray was first discretized into three compartments (of nearly similar area fraction) along the main liquid flow direction. The compartment boundaries were aligned with the orthogonally arranged planes along the tap locations (refer to the model scheme in Table 1 and tap locations in Figure 4 (top middle)). For each operating condition, the conductivity profiles along compartment boundaries were averaged according to Eq. (9), and the RTD function and its parameters for each compartment were acquired via deconvolution using axial dispersion model as exactly followed for the entire tray in Section 3.1. Very high liquid backmixing in the first compartment as indicated by a Péclet number below unity (not shown here) was observed for each condition. This was problematic as the area under the respective RTD function did not equate unity possibly because of the excessive liquid fluctuations at the inlet of that compartment [66]. Therefore, hydrodynamic and performance data of the first compartment were discarded from the whole campaign, and the data from the other two compartments constituting a ‘*modified tray*’ (as shown in Figure 5 (top left)) were considered for the model validation. Further explanation on the behavior of the first compartment can be found elsewhere [24].

Moving on to the *modified tray*, both compartments had nearly similar area fractions and their gas allocation indices were assumed unity. For each operating condition, similar liquid backmixing and residence times were observed in the compartments of the *modified tray* (see Figure 5 (top right)), and hence, the compartment efficiencies did not vary strongly. Figure 5 (bottom) also summarizes the performance data gathered by applying the exact procedure outlined in Section 3.2.2 on concentration distributions of the *modified tray*. The efficiency predictions from the RRTD model (Eq. (8)), RTD model (Eq. (7)) and AIChE model (Eq. (5)) based on the

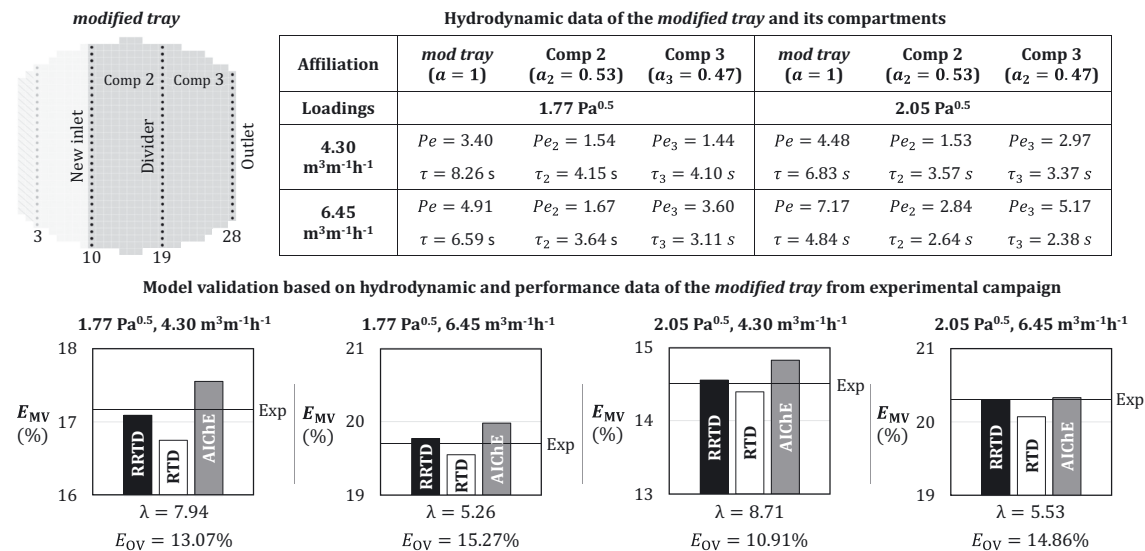


Figure 5: Hydrodynamic and performance data of a *modified tray* and its compartments including predictions from the tray efficiency models for the given operating conditions.

hydrodynamic and performance data of the *modified tray* are shown in Figure 5 (bottom) along with the tray efficiencies obtained experimentally. High liquid backmixing, low liquid diffusivity, uniform liquid velocities (refer to Figure 3b (left)) and gas plug flow in the compartments collectively led to low efficiencies with very small distinctions in the model predictions. Among those predictions, the RRTD model provided the best estimates of the tray efficiency. On the other hand, the RTD model and the AIChE model underpredicted and overpredicted the tray efficiencies respectively, and the latter is known for that in the literature [11]. Further extrapolation of the model efficiencies based on hydrodynamic data for the given operating conditions are available separately [24]. Although these results validated the accuracy of the RRTD model, more evidence was needed to showcase its supremacy over the other models as illustrated below.

4.2 Model assessment based on additional case studies

To justify the superiority of the RRTD model, significant variations in the liquid flow characteristics in the compartments (with different degrees of liquid backmixing) and non-uniform gas flow through the tray are required. Since this is very challenging to fulfil experimentally, two independent cases studies were considered to examine the promise of the RRTD model. The cases studies further allow considering different distributions of the complementary performance data in the model analysis unlike experiments. A full description of the case studies is available elsewhere [19], while only the highlights of those are briefly revisited to support the claims of the RRTD model.

The first case study focused on analyzing the impact of local liquid flow characteristics on the overall tray efficiency. In that case study, the tray was discretized into two identical and independent compartments with uniform gas flow. To apply any conventional tray efficiency model, the RTD function and its parameters were assumed for the entire tray as shown in Figure 6a (left). The RTD model was selected as a representative of the conventional models, and its predictions are presented in Figure 6a (right). For this purpose, the complementary performance data via combined values of the dimensionless group λE_{OV} were assumed, which is a common practice for model examinations in the literature [11]. The upper limit of the tray efficiency from the plug flow model is also provided in Figure 6a (right). Then, three separate cases (A–C) with liquid flow characteristics significantly different from each other were subjected to the RRTD model application. Those characteristics (i.e., represented by the RTD parameters) were identical in the compartments in Case A, whereas non-identical characteristics in the compartments with significant variations from each other were considered independently in Cases B and C (see Figure 6a (left)). It is worth mentioning that the convolution integral of the liquid RTD functions pertaining to the compartments in each case was the same as the overall liquid RTD function of the tray. In each case, the liquid flow in the compartments also confirmed the additive properties of the mean residence times and variances (not shown here). The essence of these mentions is that the overall liquid flow characteristics remained identical in each case irrespective of the local variations in the compartments, and hence, the RTD model efficiencies remained unchanged for these cases. Figure 6a (right) also shows the efficiency predictions from the RRTD model for these cases. In this figure, the RRTD model predictions from Case A and the RTD model predictions are nearly identical. This comparison indicates that the conventional tray models consider a tray to be composed of equisized compartments with identical flow behavior of liquid and gas phases. These conditions were also manifested in the experimental campaign in Section 4.1, which explains the minor variations in efficiency predictions. On the other hand, higher and lower efficiency ratios compared to Case A can be seen in Cases B and C, respectively in Figure 6a (right). For any given λE_{OV} in Case B, the efficiency ratio of the first compartment approached that of the plug flow model due to high Péclet number. Combining the efficiency ratio of the first compartment and that of the second compartment (with moderate liquid backmixing) using the RRTD model resulted in the overall efficiency ratio higher than that of Case A (or the RTD model) in Figure 6a (right). Similarly, for any given λE_{OV} in Case C, the efficiency ratio of the first compartment was almost equal to unity due to very high liquid backmixing there. Combining the efficiency ratio of the first compartment and that of the second compartment (with moderate liquid backmixing) using the RRTD model resulted in the overall efficiency ratio lower than that of Case A (or the RTD model) in Figure 6a (right). More details in this regard are available

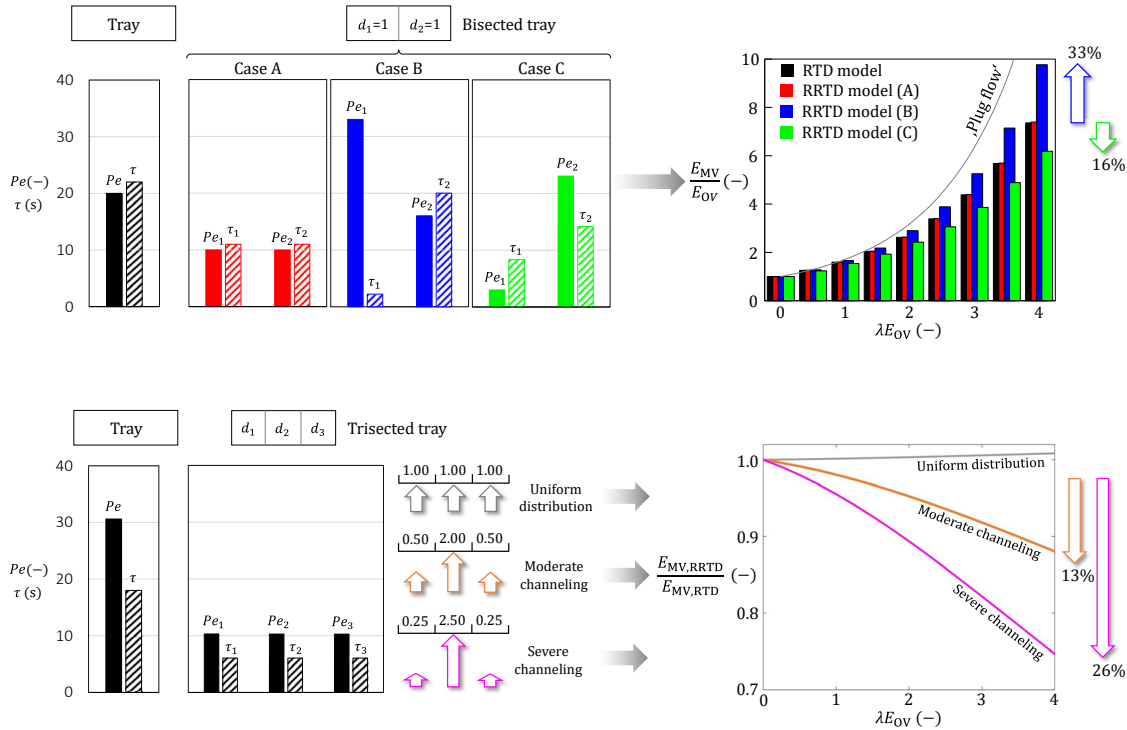


Figure 6: Case studies justifying the promise of the RRTD model by separately analyzing the impacts of (a) local flow variations in the liquid phase and (b) gas flow maldistributions on the tray efficiencies.

elsewhere [19]. With respect to Case A, the maximum variations in the efficiency ratios from Cases B and C are visible at the highest λE_{OV} in Figure 6a (right). These observations certify that the RRTD model can account for the effects of local variations in the liquid flow over a tray thereby finally breaking the convention of the black-box efficiency estimation.

In the second case study, the impact of gas flow maldistribution on the overall tray efficiency was investigated. For that purpose, the tray was partitioned into three equisized compartments with identical liquid flow characteristics such that the convolution integral of the liquid RTD functions from the compartments equated to the overall liquid RTD function from the tray. The additive properties of the mean residence times and variances from the compartments were also held in this case study. These characteristics were deliberately selected so that the predictions from the RRTD model and the RTD model were nearly identical for the uniform distributed gas plug flow over the tray (see Figure 6b (left)). Then, the variations in the gas flow profiles (i.e., referred to as moderate and severe channeling in Figure 6b (left)) were considered in the model application such that the overall gas flow through the tray remained unchanged. Figure 6b (right) confirms that the gas flow maldistribution is detrimental to the tray efficiency, and the efficiency loss is proportional to the degree of maldistribution. As shown in this figure, significant efficiency penalties are associated with the gas flow maldistributions particularly at the highest λE_{OV} .

It is worth reminding that separate impacts of liquid and gas flow maldistributions were examined in these case studies. Excessive hydraulic gradients pertaining to liquid phase on the trays can be precursors to vapor flow maldistributions, and vice-versa [22]. Thus, an industrial column would typically have flow non-idealities coexisting in both phases, and the combined efficiency losses would be worse than those shown in the case studies. Such losses can be accurately predicted by the RRTD model application making it superior to the conventional tray efficiency models.

5 Conclusions

This work presented the proof of concept of the recently proposed RRTD model that significantly advances the state of the art of the tray efficiency prediction models. Validating the RRTD model demanded full description of the two-phase flow and mass transfer on a representative large-scale column tray. The discussion on the multifaceted challenges involved in acquiring the relevant data in high resolution explained their previous unavailability in literature. To acquire such data and propose a constructive framework for model validation, a comprehensive experimental campaign was performed that involved an operational air-water column simulator along with a recently patented flow profiler, new chemical system, and novel data processing algorithms. By complementing the campaign data with results from numerical case studies, the promise of the RRTD model was demonstrated. This model finally broke the convention of the black-box estimation of the tray efficiencies by the existing models. This model can also quantify the impact of vapor flow maldistribution on the tray efficiency unlike any other model. Further spatial discretization in the directions normal to that of the main liquid flow will conceptually improve the prediction capabilities of the RRTD model. Having non-uniform distributions of point efficiency, liquid entrainment and weeping among tray compartments will involve more real-world particularities in the performance assessment of column trays. The learnings from this work are particularly useful for planning future campaigns to evaluate realistic performances of column trays as well as those of the tray efficiency models. This campaign will be particularly useful for investigating hydrodynamic and mass transfer performance of different tray designs (including high-performance valve trays, trays with flow promotion devices, etc.). In case of unavailability of sophisticated measurement techniques, this work encourages discretizing a tray by strategically placing convenient point measurement probes and sampling taps at preselected compartment boundaries and obtaining hydrodynamic and performance data for the RRTD model application. The data processing schemes presented in this work can be adapted to other measurement techniques for analyzing two-phase flow and mass transfer in a similar fashion. Furthermore, industrial columns typically monitor column-wise distributions of tray efficiency based on liquid sampling at tray boundaries. Having an RRTD model-led numerical framework for an industrial column (like that in case studies) will allow identifying potential liquid and vapor flow maldistributions for a given tray efficiency thereby assisting in column troubleshooting. Besides, the acquired data in this work also serves as a new benchmark for detailed validations of CFD and efficiency prediction models.

Research ethics: Not applicable.

Informed consent: Not applicable.

Author contributions: All authors have accepted responsibility for the entire content of this manuscript and approved its submission.

Use of Large Language Models, AI and Machine Learning Tools: None declared.

Conflict of interest: The authors state no conflict of interest.

Research funding: German Academic Exchange Service (Deutscher Akademischer Austauschdienst, DAAD, grant number: 91563198) (Vineet Vishwakarma) Erasmus+ program of the European Union (Sara Marchini).

Data availability: The raw data can be obtained on request from the corresponding authors.

References

1. Kooijman HA, Sorensen E. Recent advances and future perspectives on more sustainable and energy efficient distillation processes. *Chem Eng Res Des* 2022. <https://doi.org/10.1016/j.cherd.2022.10.005>.
2. Górak A, Olujic Z. *Distillation: equipment and processes*. Academic Press; 2014.
3. Olujic BK, Jansen H, Rietfort T, Zich E, Frey G. Distillation column internals/configurations for process intensification. *Chem Biochem Eng Q* 2003;17:301.
4. Sholl DS, Lively RP. Seven chemical separations to change the world. *Nature* 2016;532:435–7.

5. Vishwakarma V, Rigos N, Schubert M, Hampel U. Efficiency estimation of tray columns based on flow profiles and vapor–liquid equilibrium characteristics of binary mixtures. *Ind Eng Chem Res* 2019a;58:23347–58.
6. Kister HZ, Haas JR., Hart DR., Gill DR. *Distillation design*. New York: McGraw-Hill; 1992.
7. Lockett M. *Distillation tray fundamentals*. New York, NY: Cambridge University; 1986.
8. Noriler D, Meier H, Barros A, Maciel MW. Thermal fluid dynamics analysis of gas–liquid flow on a distillation sieve tray. *Chem Eng J* 2008; 136:133–43.
9. Schubert M, Piechotta M, Beyer M, Schleicher E, Hampel U, Paschold J. An imaging technique for characterization of fluid flow pattern on industrial-scale column sieve trays. *Chem Eng Res Des* 2016;111:138–46.
10. Li Y, Wang L, Yao K. New technique for measuring fluid flow patterns on a multiple downcomer tray. *Ind Eng Chem Res* 2007;46:2892–7.
11. Vishwakarma V, Schubert M, Hampel U. Assessment of separation efficiency modeling and visualization approaches pertaining to flow and mixing patterns on distillation trays. *Chem Eng Sci* 2018;185:182–208.
12. Luo N, Qian F, Ye Z-C, Cheng H, Zhong W-M. Estimation of mass-transfer efficiency for industrial distillation columns. *Ind Eng Chem Res* 2012;51:3023–31.
13. Lewis J, W. *Rectification of binary mixtures*. *Ind Eng Chem* 1936;28:399–402.
14. Gerster JA, Hill AB, Hochgraf NN, Robinson DG. *Tray efficiencies in distillation columns - final report from the University of Delaware*. American Institute of Chemical Engineers (AIChE) 1958. Newyork, NY.
15. Gautreaux, MF, O'Connell, HE. Effect of length of liquid path on plate efficiency; 1953.
16. Foss AS, Gerster J, Pigford R. Effect of liquid mixing on the performance of bubble trays. *AIChE J* 1958;4:231–9.
17. Ashley M, Haselden G. The calculation of plate efficiency under conditions of finite mixing in both phases in multiplate columns, and the potential advantage of parallel flow. *Chem Eng Sci* 1970;25:1665–72.
18. Bell RL. Residence time and fluid mixing on commercial scale sieve trays. *AIChE J* 1972;18:498–505.
19. Vishwakarma V, Schubert M, Hampel U. Development of a refined RTD-based efficiency prediction model for cross-flow trays. *Ind Eng Chem Res* 2019b;58:3258–68.
20. Górak A, Sorensen E. *Distillation: fundamentals and principles*. Academic Press; 2014.
21. Lockett M, Dhulesia H. Murphree plate efficiency with nonuniform vapour distribution. *Chem Eng J* 1980;19:183–8.
22. Mohan T, Rao KK, Rao DP. Effect of vapor maldistribution on tray efficiency. *Ind Eng Chem Process Des Dev* 1983;22:376–80.
23. Furzer I. The effect of vapor distribution on distillation plate efficiencies. *AIChE J* 1969;15:235–9.
24. Vishwakarma V. Experimental and numerical investigations for an advanced modeling of two-phase flow and mass transfer on column trays. TU Dresden; 2022.
25. Bennett DL, Kao AS, Wong LW. A mechanistic analysis of sieve tray froth height and entrainment. *AIChE J* 1995;41:2067–82.
26. Gesit G, Nandakumar K, Chuang KT. CFD modeling of flow patterns and hydraulics of commercial-scale sieve trays. *AIChE J* 2003;49: 910–24.
27. Hirschberg S, Wijn E, Wehrli M. Simulating the two phase flow on column trays. *Chem Eng Res Des* 2005;83:1410–24.
28. Marchini S, Vishwakarma V, Schubert M, Brunazzi E, Hampel U. Direct tray and point efficiency measurements including weeping effects through a convenient add-on for air–water simulators. *Ind Eng Chem Res* 2021;60:2600–12.
29. Vishwakarma V, Schleicher E, Bieberle A, Schubert M, Hampel U. Advanced flow profiler for two-phase flow imaging on distillation trays. *Chem Eng Sci* 2021b;231:116280.
30. Bernard J, Sargent R. The hydrodynamic performance of a sieve plate distillation column. *Trans Inst Chem Eng* 1966;44:T314.
31. D'Arcy, D. Analysis of sieve tray froths such as occur in heavy water production plants; 1978.
32. Hofhuis, PAM. Flow regimes on sieve-trays for gas/liquid contacting; 1980.
33. Pinczewski W, Fell C. Nature of 2-phase dispersion on sieve plates operating in spary regime. *Trans Inst Chem Eng* 1974;52:294–9.
34. Raper JA, Kearney M, Burgess J, Fell C. The structure of industrial sieve tray froths. *Chem Eng Sci* 1982;37:501–6.
35. Val Pinczewski W, Benke ND, Fell CJ. Phase inversion on sieve trays. *AIChE J* 1975;21:1210–13.
36. Abdullah J. Gamma-ray scanning for troubleshooting, optimization and predictive maintenance of distillation columns. *Hydrocarb Asia* 2005;1:62–5.
37. Aquino DD, Mallillin JP, Sulit RF, Hila FC, Nuñez IAA, Bulos AD. Performance evaluation of a rectifier column using gamma column scanning. *Nukleonika* 2017;62:285–7.
38. Gorak A, Schoenmakers H. *Distillation: operation and applications*. Academic Press; 2014.
39. Haraguchi MI, Calvo WAP, Kim HY. Tomographic 2-D gamma scanning for industrial process troubleshooting. *Flow Meas Instrum* 2018; 62:235–45.
40. Burgess J, Calderbank P. The measurement of bubble parameters in two-phase dispersions—I: the development of an improved probe technique. *Chem Eng Sci* 1975;30:743–50.
41. Hu B, Yang H, Hewitt GF. Measurement of bubble size distribution using a flying optical probe technique: application in the highly turbulent region above a distillation plate. *Chem Eng Sci* 2007;62:2652–62.
42. Solari R, Bell R. Fluid flow patterns and velocity distribution on commercial-scale sieve trays. *AIChE J* 1986;32:640–9.
43. Yu K, Huang J, Li J, Song H. Two-dimensional flow and eddy diffusion on a sieve tray. *Chem Eng Sci* 1990;45:2901–6.
44. Porter K, Lockett M, Lim C. The effect of liquid channelling on distillation plate efficiency. *Trans Inst Chem Eng* 1972;50.
45. Biddulph MW, Bultitude DP. Flow characteristics of a small-hole sieve tray. *AIChE J* 1990;36:1913–16.
46. Stichlmair J, Ulbrich S. Liquid channelling on trays and its effect on plate efficiency. *Chem Eng Technol* 1987;10:33–7.

47. Liu C, Yuan X, Yu KT, Zhu X. A fluid–dynamic model for flow pattern on a distillation tray. *Chem Eng Sci* 2000;55:2287–94.
48. Porter K, Yu K, Chambers S, Zhang M. Flow patterns and temperature profiles on a 2.44 m diameter sieve tray. *Chem Eng Res Des* 1992;70:489–500.
49. Zhimin S, Chunjiang L, Guocong Y, Xigang Y. Prediction of distillation column performance by computational mass transfer method. *Chin J Chem Eng* 2011;19:833–44.
50. Nutter DE. Ammonia stripping efficiency studies. In: Presented at the AIChE. Symp. Ser.; 1972:68 p.
51. Lockett, M, RD, K, Ms, U. Froth regime point efficiency for gas-film controlled mass transfer on a two-dimensional sieve tray; 1979.
52. Lockett, M, Uddin, M. Liquid-phase controlled mass transfer in froths on sieve trays; 1980.
53. Lamprecht, JH. The development of simplistic and cost-effective methods for the evaluation of tray and packed column efficiencies; 2017.
54. Prado M, Fair JR. Fundamental model for the prediction of sieve tray efficiency. *Ind Eng Chem Res* 1990;29:1031–42.
55. Garcia JA, Fair JR. A fundamental model for the prediction of distillation sieve tray efficiency. 1. Database development. *Ind Eng Chem Res* 2000;39:1809–17.
56. Yanagi T, Sakata M. Performance of a commercial scale 14% hole area sieve tray. *Ind Eng Chem Process Des Dev* 1982;21:712–17.
57. Lockett M, Ahmed I. Tray and point efficiencies from a 0.6 metre diameter distillation column. *Chem Eng Res Des* 1983;61:110–18.
58. Hampel U, Schubert M, Döb A, Sohr J, Vishwakarma V, Repke J-U, et al. Recent advances in experimental techniques for flow and mass transfer analyses in thermal separation systems. *Chem Ing Tech* 2020;92:926–48.
59. Manivannan RG, Cai T, McCarley K, Vennavelli A, Aichele CP. Evaluation of the validity of tray and point efficiency correlations at elevated liquid viscosities and proposal of an improved point efficiency correlation. *Chem Eng Res Des* 2020;159:27–35.
60. Bennett D, Agrawal R, Cook P. New pressure drop correlation for sieve tray distillation columns. *AIChE J* 1983;29:434–42.
61. Vishwakarma V, Haq SA, Schleicher E, Schubert M, Hampel U. Experimental analysis of the hydrodynamic performance of an industrial-scale cross-flow sieve tray. *Chem Eng Res Des* 2021a;174:294–306.
62. Vishwakarma, V, Schleicher, E, Schubert, M, Tschofen, M, Löschau, M, 2020. Sensor zur Vermessung von Strömungsprofilen in großen Kolonnen und Apparaten (English translation: Sensor for measuring flow profiles in large columns and apparatus). DE102018124501.
63. Prasser H-M, Böttger A, Zschau J. A new electrode-mesh tomograph for gas–liquid flows. *Flow Meas Instrum* 1998;9:111–19.
64. Vishwakarma V, Wiedemann P, Schleicher E, Schubert M, Hampel U. A new approach for estimating the effective froth height on column trays. *Chem Eng Sci* 2021c;231:116304.
65. Marchini S, Vishwakarma V, Schubert M, Brunazzi E, Hampel U. Effects of non-uniform weeping distributions on tray and point efficiencies. *Results Eng* 2023;19:101238.
66. Levenspiel O. *Chemical reaction engineering*. John Wiley & Sons; 1998.